Graphical Facial Expression Analysis and Design Method: An Approach to Determine Humanoid Skin Deformation

Yonas Tadesse[1,2]
e-mail: yonas@vt.edu;
yonas.tadesse@utdallas.edu

Shashank Priya
e-mail: spriya@vt.edu

Center for Energy Harvesting
Materials and Systems (CEHMS),
Bio-Inspired Materials and
Devices Laboratory (BMDL),
Center for Intelligent Material
Systems and Structure (CIMSS),
Department of Mechanical Engineering,
Virginia Tech,
Blacksburg, VA 24061

The architecture of human face is complex consisting of 268 voluntary muscles that perform coordinated action to create real-time facial expression. In order to replicate facial expression on humanoid face by utilizing discrete actuators, the first and foremost step is the identification of a pair of origin and sinking points (SPs). In this paper, we address this issue and present a graphical analysis technique that could be used to design expressive robotic faces. The underlying criterion in the design of faces being deformation of a soft elastomeric skin through tension in anchoring wires attached on one end to the skin through the sinking point and the other end to the actuator. The paper also addresses the singularity problem of facial control points and important phenomena such as slacking of actuators. Experimental characterization on a prototype humanoid face was performed to validate the model and demonstrate the applicability on a generic platform. [DOI: 10.1115/1.4006519]

Keywords: humanoid prototype, facial expression, artificial skin, contractile actuator, graphical analysis

1 Introduction

Facial expression of humanoid is becoming a key research topic in recent years in the areas of social robotics. The embodiment of robotic head akin to that of human being promotes a more friendly communication between the humanoid and the user. There are many challenges in realizing human-like face such as material suitable for artificial skin, muscles, sensors, supporting structures, machine elements, vision, and audio systems. In addition to materials and their integration, computational tools, static and dynamic analysis are required to fully understand the effect of each parameter on the overall performance of a prototype humanoid face and provide optimum condition.

This paper is organized in eight sections. First, we introduce the background and methodology for creating facial expression in robotic heads. A thorough description of the overall problem associated with expression analysis is presented along with pictorial representation of the muscle arrangement on a prototype face. Second, a literature survey is presented on facial expression analysis techniques applied to humanoid head. Third, the description of graphical facial expression analysis and design (GFEAD) method is presented focusing on two generic cases. Fourth, application of the GFEAD method on a prototype skull is presented and important manifestations that could not be obtained with other techniques are discussed. Fifth, results from experimental characterization of facial movement with a skin layer are discussed. Sixth, the effect of the skin properties and associated issues will be discussed. Section 7 discusses the significance of GFEAD method on practical platforms. Finally, the summary of this study is presented in Sec. 8.

In the last few years, we have demonstrated humanoid heads using a variety of actuation technologies including: piezoelectric ultrasonic motors for actuation and macrofiber composite for sensing [1]; electromagnetic RC servo motor for actuation and embedded unimorph for sensing [2,3], and recently shape memory alloy (SMA) based actuation for baby humanoid robot focusing on the face and jaw movement [4]. We have also reported facial muscles based on conducting polymer actuators to overcome the high power requirement of current actuation technologies including polypyrrole–polyvinylidene difluoride composite stripe and zigzag actuators [5] and axial type helically wounded polypyrrole–platinum composite actuators [6]. All these studies have identified the issues related to the design of facial structure and artificial muscle requirements. Other types of actuators such as dielectric elastomer were also studied for general robotics application [7].

There are several other studies reported in literature related to humanoid facial expression. Facial expression generation and gesture synthesis from sign language has been applied in the animation of an avatar [8], expressive humanoid robot Albert-HUBO with 31 *Degree of Freedom (DOF)* head and 35 DOF body motions based on servo motors [9], facial expression imitation system for face recognition and implementation on mascot type robotic system [10], facial expressive humanoid robot SAYA based on McKibben pneumatic actuators [11], and android robot Repliee for studying psychological aspects [12]. However, none of these studies address the design strategy for humanoid head based on discrete actuators. Computational tools for precise analysis of the effect of actuator arrangement on the facial expression are missing.

Even though significant efforts have been made, there is little fundamental understanding of the structural design questions. How these facial expressions can be precisely designed? How are the terminating points on the skull determined? What will be the effect of variation in arrangement of actuators? The answer to these questions requires the development of an accurate mathematical model that can be easily coded and visualized. For this purpose, we present a GFEAD method for application in humanoid head development. This method will be briefly discussed for generic cases to illustrate all the computational steps.

The prime motivation behind using the graphical approach is that it provides both visual information as well as quantitative data required for the design and analysis of humanoid face. The deformation analysis and design is performed directly on the skull surface, which ultimately forms the platform for actuation. The graphical approach is simple to implement as it is conducted in 2D. Generally, the skull is created from a scanned model; thus,

[1]Present address: Mechanical Engineering Department, University of Texas at Dallas 800 West Campbell Rd., Richardson, TX 75080.
[2]Corresponding author.

Contributed by the Mechanisms and Robotics Committee of ASME for publication in the Journal of Mechanisms and Robotics. Manuscript received October 10, 2010; final manuscript received February 23, 2012; published online April 25, 2012. Assoc. Editor: Qiaode Jeffrey Ge.

millions of points are spatially generated and meshed to form 3D skull in a *Computer Aided Design (CAD)* program [13,14]. Creating mechanical structure by itself in the solid model is difficult unless the resolution is reduced. Thus, visualization for various actions is quite cumbersome and computationally expensive. The graphical approach provides solution to this problem and also 2D surfaces to conduct visualization and optimization. Graphical representation has several advantages in the design of robotic face as compared to analytical models because it reduces the assumption involved in computation, does not require actuator model, and can easily account for the elastomeric skin variables. The good example is the slacking phenomena that will be discussed in Sec. 4 and Fig. 5. One cannot easily determine the behavior of actuator in the analytical method especially for multiple actuators connected at a control point. Another good example is that of inverse problem, case II, which will be discussed in Sec. 3.2. Analytical method will be difficult to select arbitrary sinking points and determine whether the given deformation is possible or not. Currently, many humanoid heads with facial expression capability have been reported in literature. However, limited discussion is presented in the literature on how one can determine the sinking points or terminating points and their effects on facial expression.

In this paper, five terms are frequently used and for clarity we define them as follows: (i) *Anchor point (AP)* is a point on the elastomeric skin that is free to move in any direction governed by the supporting structure underneath and the actuator attached; (ii) *SP* is a point on the artificial skull where the contractile actuator or muscle passes or terminates; (iii) *Action unit (AU)* is an element which is responsible for the face deformation. It is a directional vector consisting of an actuator with an anchor point as origin and directed to a sinking point; (iv) *Principal plane* is an orthographic plane that shows either the front, bottom, or side view of the skull and is represented by a capital letter in a square bracket such as [F] and [B]; and (v) *Auxiliary view* is an orthographic view projected from adjacent orthographic view. A square bracket ([A1], [A2]) is used as its symbol.

To illustrate a human-like complex facial expression, the anchor points on the face need to be actuated sequentially or independently. The location of sinking points (terminating points) of the actuator needs to be selected appropriately as this determines the facial emotion on the face of the robot. It has been shown in literature [15–17] that action units on human face lay close to facial features such as tip of the mouth, nose, edge of cheek muscle, frontal eyebrow, etc. A number of humanoid robots adapted the AUs from the facial action coding system (FACS). Therefore, the origin of action units (anchor points) can be chosen in the vicinity of facial features. However, a more precise method for identifying the position of sinking point as well as a good control of the direction of movement is desired. This paper investigates the method for determining the sinking points that control the direction of facial movement and the effect of various arrangements of actuators in 2D plane. It is worthwhile to mention that a combination of geometries such as isosceles triangle and trapezoidal pivots for flexural structure provide desired properties of a compliant joint as demonstrated in Ref. [18]. In a similar manner, triangles that are constructed using anchor points and sinking points provide several advantages in studying the effect of various combinations of actuators in the GFEAD method.

GFEAD will be useful to develop an expressive humanoid face platform using computational graphical techniques. The graphical method of analysis provides a systematic approach in selecting and identifying the crucial points and thus has inherent advantage in the design of robotic faces. GFEAD method uses auxiliary views to observe the movement of contractile actuator in true shape and its direction of action. If control points are attached in different configuration such as multiple connection points from action units, the facial movement will be different. In most cases, the direction and magnitude of facial movement cannot be seen in the principal plane of view (front or side). Therefore, auxiliary views are needed to see the exact movement of action units. The auxiliary views are orthographic views taken from a direction of sight other than the conventional top, front, right side, left side, bottom, or rear view. Primary auxiliary views ([A1]) are projected onto a plane that is perpendicular to only one of the principal planes of projection and is inclined to the other two planes at certain angle. Secondary auxiliary ([A2]) views are projected from primary auxiliary views.

The humanoid prototype head used for investigation utilizes contractile type of actuator, Biometal fiber SMA wire. Biometal fiber is commercially available from Toki Corp., Japan. The robotic head was constructed using artificial skull as a support structure, SMA routing pulleys, two firewire CMOS camera, elastomeric skin, and battery powered microcontroller based driving circuit [4]. The artificial skull was made from Acrylonitrile butadiene styrene (ABS) plastic on which elastomeric artificial skin was attached. Inside the skull, several pulleys for routing the SMA wires were mounted and the SMAs were connected to the skin via the sinking points. Figure 1(*a*) illustrates the architecture of robotic head including interconnection of artificial skin, attachment of contractile actuator to anchor points, and routing of actuator through sinking points on the skull and pulley systems. Figure 1(*b*) shows the assembled prototype as seen from the back side and Fig. 1(*c*) is the front view of the robotic head. When the actuators are activated with microcontroller sequentially or independently, the anchor points (control points) move in a specific direction prescribed by the arrangement of actuators on the skull, thereby deforming the elastomeric skin. This results in facial expression in the face robot.

2 Facial Expression Analysis Techniques

Prior research on the design of facial expressions has mainly focused on computational algorithms and programs such as gesture synthesis from a sign language for animated humanoid [8], synthesis of images from audio and video for virtual reality [19], interaction between human and humanoid accounting for the reaction to a subject group [20–22], and a model of mascot face based on transformation matrix between an affect space and face [23,24]. There has been emphasis on the implementation of these techniques for pre-eminent interaction between a human and machine interface [25–28]. Several efforts have been made to develop a facially expressive humanoid robot in various laboratories. However, limited information was provided on the methodology for design of human-like faces using artificial actuators and some of the techniques presented are more appropriate for mascot type robots. Construction of 3D face from 2D portrait manipulation by using a prerecorded facial motion database and generating the corresponding 3D facial expressions were presented in Ref. [29]. Mapping of facial emotion from a human to humanoid robots was found to be effective for generation of facial features in autonomous robotic systems [30]. However, such approaches do not contribute in design of artificial facial expression on humanoids.

A number of studies enable us to understand facial expression in human beings of diverse ethnicity. FACS developed by Ekman and Friesen in 1978 provides us the basics of facial expression. Carnegie Mellon researchers have developed comprehensive action unit coded image database including 2105 digitized images from 182 adult subjects that perform multiple actions from the primary FACS action units [15]. Automatic face analysis system [31] provided us a useful tool to understand and analyze facial expressions based on both permanent facial features (brows, eyes, mouth) and transient facial features (deepening of facial furrows) in a nearly frontal-view image sequence. One of the interesting works based on finite element based model combined anatomical facial muscle structure with physical model of human face [32]. The finite element based model formulates a second order discrete differential equation to simulate facial tissue using a hexahedral deformable lattice element. Another approach following parametric normalization and deformation schemes has been proposed to generate facial expression for robotic head system with high

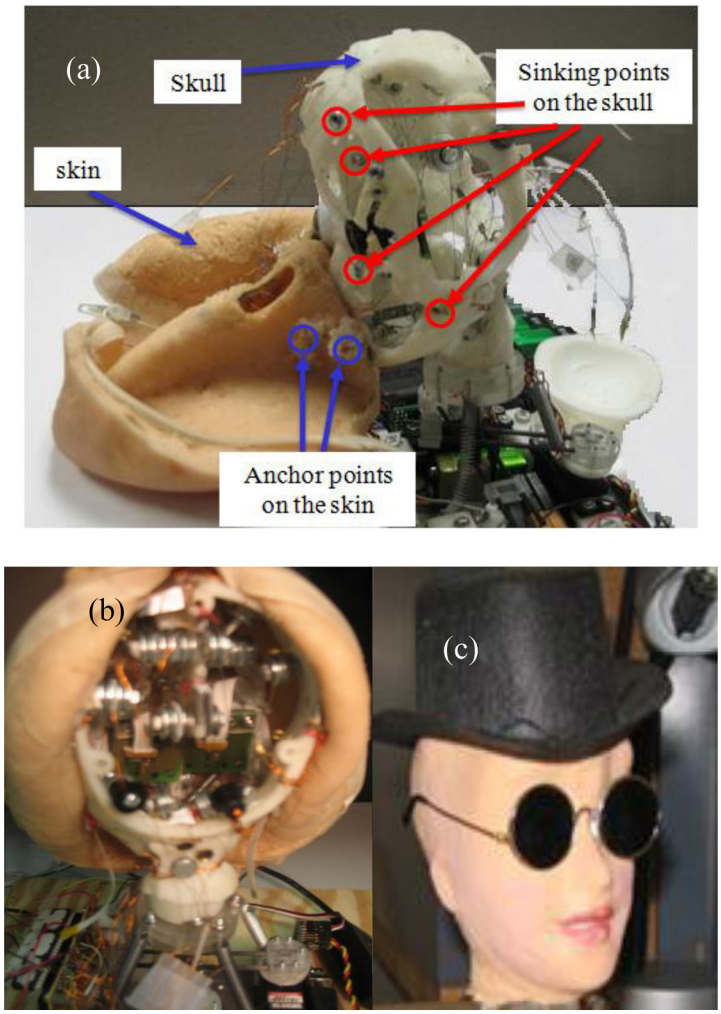

Fig. 1 Baby humanoid face: (*a*) architecture of skin–actuator-structure interconnection, (*b*) back-side view after assembly, and (*c*) front view after assembly

recognition rate [33]. In this case, the percentage change of facial features with respect to normal feature positions was taken as a normalized parameter to quantify various expressions. A kinematics based model with revolute and prismatic joints has been used to show the six basic facial expressions through simulations of a character face.

Singularity in a robotic mechanism or robotic manipulator is a major concern and several researchers have investigated this issue including a 3-Revolute-Prismatic-Revolute (RPR) mechanism closeness to singularity by Hubert and Merlet [34]; singularity analysis for deformable closed contour by Myszka et al. [35]; and different kind of singularities observed in serial, parallel, and hybrid mechanisms by Park and Kim [36]. Similarly, in the design of facial expressive humanoid robot head, some sort of computational tools are required to unravel most of the issues associated in the design as well as analysis of facial expression applied to prototype face.

Implementation of facial expression on humanoid robots has several challenges. Previously, humanoid head with flexible face film and dc motor as a main actuator element along with supporting mechanical systems has been presented [37]. The authors discussed about the properties of the skin such as flexibility, anti-aging, anticracking, and coloring. Fourteen action units were chosen from FACS to demonstrate the facial expression in the portrait humanoid [37]. To minimize the number of actuators, grouping the muscle types has been proposed. Minimization of actuators is useful in the design of humanoid face particularly for large actuation system such as motors and pneumatic actuators [38]. A cam mechanism and electric motors for humanoid face have been presented to optimize the actuation of facial control points. Important elements such as flexible skin, mechanical systems, deriving systems, and controllers were described with respect to actuation of the facial expression [39]. The action units described in most humanoids uses one to one correspondence between the control points and the sinking points. However, in the GFEAD method, one can control the magnitude and direction of the action units by using multiple sinking points and study the deformation behaviors on 2D plane. The 2D plane provides the actual deformation in actuator space and the corresponding deformation in the frontal view of the face robot by reprojecting the control points (back propagation). The choice of sinking points using the techniques such as GFEAD will help the ongoing research in artificial muscles using smart materials such as electroactive polymers. The direct way of selecting sinking points (or terminating points) of actuators is in the direction of the action units. But this arrangement restricts the facial movement to be in only one direction [40].

3 GFEAD Method and Step by Step Description

The analysis and design of facial expressive prototype can be done graphically in a two-dimensional plane. The method basically formulates successive auxiliary planes to find the exact plane

in which the facial control points are located. Once the orthogonal plane holding the control point and action units with their exact length have been identified, the effect of each SMA actuators (or any other contractile actuator) attached to control point can be analyzed. The analysis can be done by observing the effect of contractile actuator independently or in combination with other actuators for displacement amplification. It can also identify the direction of movement in auxiliary plane and provide its projection in the frontal plane of the face.

Two cases are presented here to illustrate the GFEAD method for the design of humanoid face and analysis—case I: Given the location of sinking points (A and B) with two actuators connected to a single anchor point on the skin (O), derive the directional control of facial movement as shown in Fig. 2(*a*), and case II: Given a desired direction of facial movement from action units with angle θ and β from reference axis as shown in Fig. 3(*a*), determine the favorable location of sinking points for two or more action units originating from an anchor point. Below, we illustrate the GFEAD method for these two cases considering step by step procedure.

Consider two views of a skull geometry utilized for support structure as shown in Fig. 2(*a*). For case I, this schematic can be simplified to that shown in Fig. 2(*b*) and suppose two SMA actuators ($\overrightarrow{OB}$ and $\overrightarrow{OA}$) originate from action unit at point "O" and pass through sinking points, "A" and "B." Further, we assume that the projection of points A and B in the frontal ([F]) plane is A_F and B_F, respectively, and the orthographic projection of A and B in the bottom plane ([B]) is A_B and B_B. The coordinate of these points can be obtained from the CAD model in the design process of the skull. Note that the actuation point that affects the facial expression is point "O." In order to find the locus of this point (action unit) when each actuator (SMA_1 and SMA_2) is activated independently or simultaneously, successive auxiliary views need to be constructed which enable identifying the plane containing the points. The procedure for both *cases I* and *II* is shown in section 3.1 and section 3.2.

3.1 Description for Case I. Figure 2(*b*) shows the partial boundaries of the skull which limits the domain of the controlling parameters. The center lines shown as S-F, F-B, and S-B represent the boundary of orthogonal planes: Side–front, front–bottom, and side–bottom, respectively. The frontal and bottom view planes are represented as [F] and [B]. Contractile actuators such as SMA are represented by arrow $\overrightarrow{OA}$ (SMA_1) and $\overrightarrow{OB}$ (SMA_2) in this figure. The position of the end points from the reference line is shown by small letters a, b, c, etc. The section below describes the step-by-step analysis of this problem.

Step I: The first auxiliary plane [A1] that provides the true length of line (O_FA_F) can be constructed by drawing a reference line (B-1) parallel to O_FA_F. By projecting a perpendicular line from the points on the [F] plane to the auxiliary plane [A1] and mapping the distances (g, h, i) from the previous auxiliary views (bottom view), the location of A_1, B_1, and O_1 can be obtained. For example, O_B and O_1 have the same distance (g unit) from reference line F-B and B-1, respectively, as shown in Fig. 2(*c*). Note that the boundary of the face curve was not projected on auxiliary plane A1 in order to reduce the complexity.

Step II: Construction of auxiliary plane ([A2]) to find the edge view of the plane $O_1A_1B_1$ or the point view of the line O_1A_1. The reference line 1–2 is perpendicular to the true length of line O_1A_1 and all the points were projected on auxiliary plane [A2] by transferring equal distance (k and j) from the front view as shown in Fig. 2(*d*).

Step III: The third auxiliary plane ([A3]) which provides us normal view of the plane $O_2A_2B_2$ (its exact shape and size) can be obtained by drawing a reference line (line 2–3) parallel to A_2B_2 and projecting the points on plane [A3]. In this plane, one can analyze the deformation due to each SMA actuator. The points A_3, O_3, and B_3 were projected using the reference line (line 2–3) and distances (m, l, and o) were transferred from the next secondary auxiliary view ([A1]) as shown in Fig. 2(*e*).

Step IV: If one of the SMA actuator is activated, the position of anchor point O_3 will be determined by the intersection of circles. For example, if only SMA_2 is activated, the position of anchor point O_3 will be determined by the intersection of the circles 1 and 2. The circles are constructed by using the radius A_3O_3 centered at A_3 and another circle with a radius of $R = B_3O_3$–4% (length of SMA_1) centered at B_3. The intersection point can be projected back on the successive auxiliary views and principal planes and then the actual deformation in the frontal and bottom plane can be obtained as illustrated in Fig. 2(*f*). The proper length of SMA actuator can be determined by considering the available space within the skull.

Step V: The intersection of the two arcs drawn in step IV provides the position of action unit in auxiliary plane [A3]. The direction of the SMA actuators is shown by the arrows O_3B_3 and O_3A_3 before the actuation and $O_{3a}B_3$ and $O_{3a}A_3$ after the actuation in Fig. 2(*g*). Since one of the SMA actuator (O_3B_3) is activated, the other one (O_3A_3) simply rotates. The total deformation of SMA actuator need not be in excess of the length O_3B_3.

Step VI: Projecting back the anchor point to auxiliary plane [A2]. Since the plane appears as a line, the action unit O_{3a} lies on line A_2B_2. The point can be projected to the first and principal plane successively by drawing a line perpendicular to the respective reference lines as shown in Fig. 2(*h*).

Step VII: The new positions of the anchor point are projected in all the planes and the respective distance from the reference axis is mapped from the previous adjacent auxiliary view as shown by black triangular marker in Fig. 2(*i*). In auxiliary plane [A1], the position of the new point O_{1a} from the reference line 1–2 is "n" unit which was mapped from plane [A3]. Similarly, the position O_{Fa} can be allocated on the frontal plane by mapping a distance "p" from auxiliary plane [A2].

Step VIII: Finally, the new position of the anchor point and the sinking points can be connected with a dashed line in the frontal view. As shown in Fig. 2(*j*), the deformation on the face can be observed as shrinkage. It should be noted here that this method assumes that the points considered (A, B, O) lie on same plane. But in practical conditions, the supporting skull structure might have a curved geometry which guides the directional movement of the facial deformation. In that condition, this method can be modified by discretization of the curved plane with triangles and using steps I–VIII.

3.2 Description of the GFEAD Method for Case II. Case II can be considered as inverse kinematics problem and stated as follows. Given desired direction (θ and β from reference line) and magnitude of muscle movement as shown in Fig. 3(*a*), determine the favorable location of sinking points with two actuators connected to a single anchor point on the skin. Furthermore, it is desired to determine the activation direction of SMA actuators for wide directional control of facial movement. This problem will be vital for optimization of the limited space in humanoid skull. Most of the procedures are similar to case I except few additional steps that will be required. This problem has been recently investigated in Ref. [40] by propagating successive auxiliary views from the frontal plane. Here, we will show the steps starting from the bottom principal plane.

Step I: The first step in this case is to take any two arbitrary points on the directional line and obtain its true length. For simplicity, one point on a directional line that does not overlap with the anchor point O and another point that coincides with the anchor point (point O). This provides a line segment with fixed length of O_FP_F in the front and O_BP_B in the bottom view as shown in Fig. 3(*b*). One might be tempted to choose the sinking point directly on the directional line. However, by doing so, one will not get the directional control of facial deformation with just one actuator.

Step II: Obtain the true length of line O_BP_B from one of the principal plane by projecting the points in the auxiliary plane [A1]

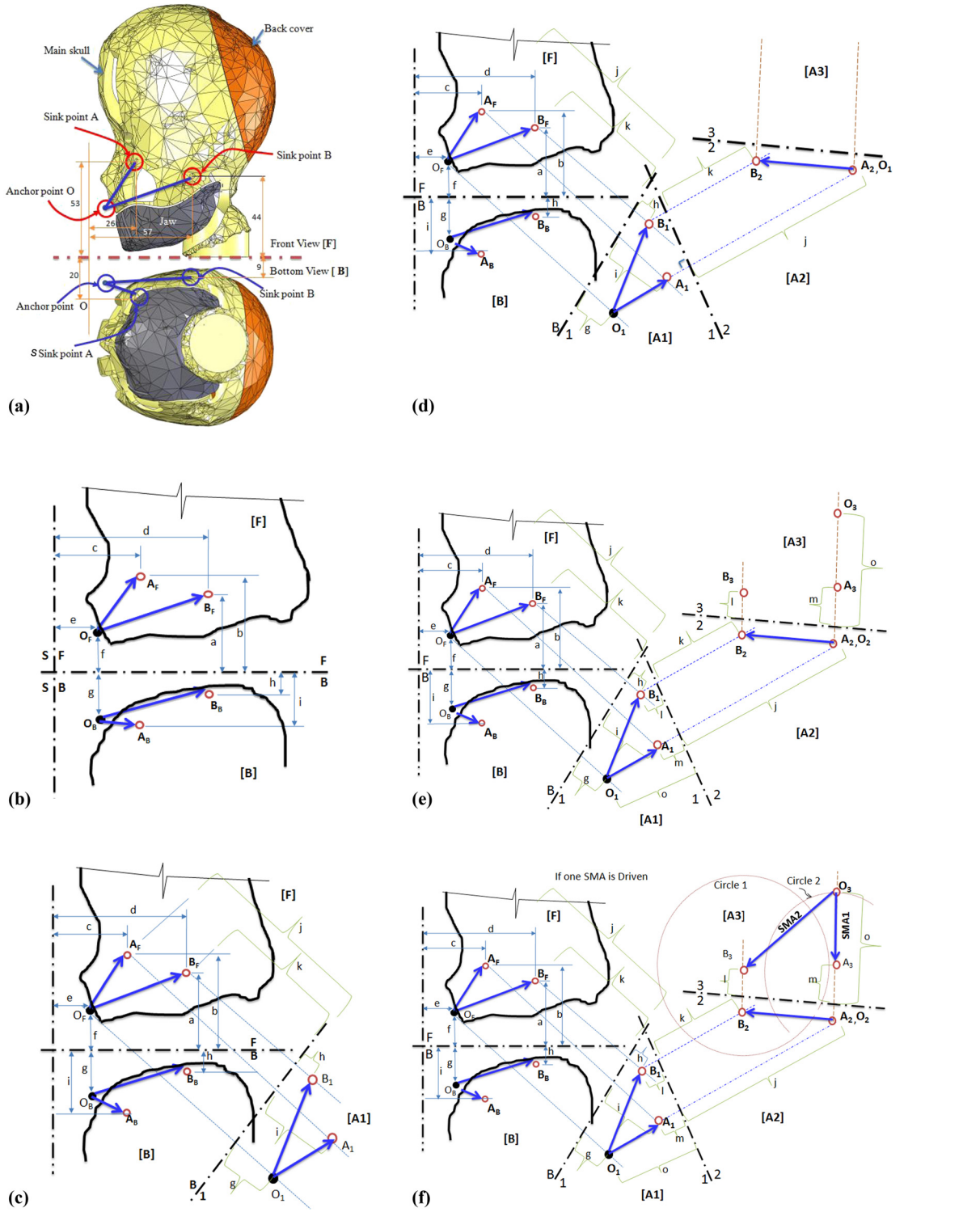

Fig. 2 Illustration of GFEAD method using contractile actuators and supporting skull structure. Steps (a)–(j) demonstrate the method for case I. (*a*) Two views of the skull showing an anchor point and two sinking points. (For convenience in analysis and to focus on the left cheek, the usually considered side view of the skull was selected to be the front view.). (*b*) Schematic diagram of the skull boundary and contractile actuators (OA = SMA_1 and OB = SMA_2). The respective distances of anchor point, sinking point, and terminating points from reference line are also shown. (*c*) *Step I*: Construction of auxiliary plane [A1] that provides the true length of OA. A reference line (B-1) is drawn parallel to O_FA_F and distances (g, h, and i) are mapped from the bottom plane [B]. (*d*) *Step II*: Construction of auxiliary plane [A2] to find the edge view of plane $O_1A_1B_1$ and introducing auxiliary plane [A3]. (*e*) *Step III*: Mapping the positions of point A_3, B_3, and O_3 on plane [A3]. The exact shape of the plane $A_3B_3O_3$ that holds the SMA actuators can be obtained on plane [A3]. (*f*) *Step IV*: Construction of circles on auxiliary plane [A3] to find the intersection points when one of the SMA_2 actuator (O_3B_3) deforms 4% and the other SMA_1 (O_3A_3) remains undeformed. (*g*) *Step V*: The position of the anchor point before actuation (O_3), after actuation (O_{3a}), and the apparent deformation ($O_{3a}O_3$) observed in auxiliary plane [A3]. (*h*) *Step VI*: Projecting back O_{3a} to the auxiliary plane [A2] to obtain O_{2a}. (*i*) *Step VII*: Propagating the position of the anchor point O_{2a} to auxiliary plane [A1] and principal plane [F]. The positions are shown with black triangular marks and named as O_{1a} and O_{Fa}. (*j*) *Step VII*: Connecting the actuated position of the anchor point O_{Fa} and the sinking points (A_F and B_F) in the frontal plane.

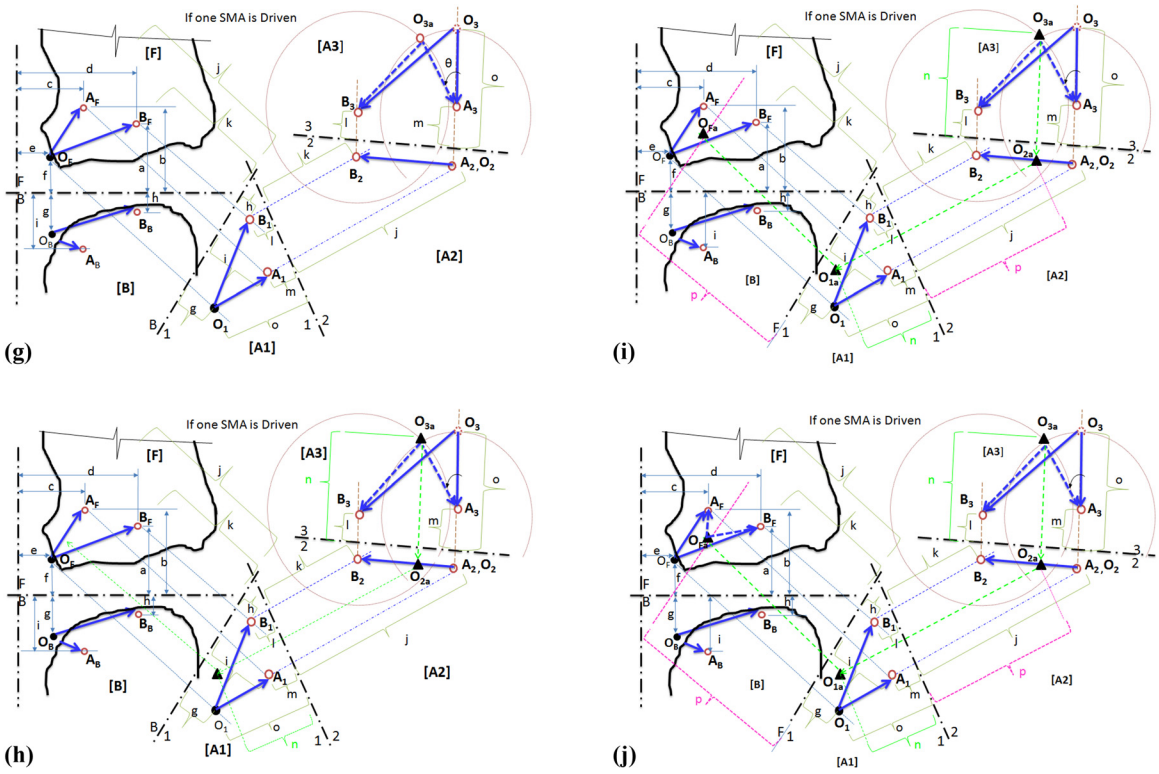

Fig. 2 (Continued).

as shown in Fig. 3(*c*). Next, obtain the point view of the line by mapping the magnitude "e" from the bottom principal plane [B] as shown in Fig. 3(*d*). The actual magnitude of deformation can be set in this auxiliary plane [A1]. This magnitude can be fixed on the line segment as indicated in Fig. 3(*d*).

Step III: In auxiliary plane [A2], one has to determine which direction the holes (sinking points) need to be located. Therefore, we construct the edge view of the plane holding the sinking points and the anchor point with angle γ with respect to reference line 1–2 as shown in Fig. 3(*e*). The angle γ can be constructed in any orientation which represents the edge view of the plane that holds all the points. This approach is quite generic. If the selected angle does not provide the favorable location of the sinking points, it can be changed iteratively and then follow the next procedure.

Step IV: Obtain the true shape of the plane that holds the sinking points and the anchor point. This is done by introducing a reference line parallel to the edge view drawn in step III and projecting the directional line in auxiliary plane [A3]. In this plane again, the true length of actual deformation "Mag" can be observed as shown in Fig. 3(*f*).

Step V: The favorable locations of sinking points can be obtained by the intersection of circles in auxiliary plane [A3]. In this case, two circles are drawn. One circle with radius R_1 centered at O_3 and another circle with radius R_2 centered at Q_3 as shown in Fig. 3(*g*). The difference between the radius R_1 and R_2 corresponds to the change in length of the SMA actuator during actuation. Different circle can be drawn by taking radius R_3 centered at O_3 and R_4 centered at Q_3 for alternative points. The only requirement for the circles is that the differences between the radii have to be equal to the desired magnitude of deformation ($\text{Mag} = R_1 - R_2 = R_3 - R_4$).

Step VI: The intersection of the arcs drawn in step V is marked for projection back to the secondary auxiliary plane [A2]. The first two candidate points obtained by intersection of arcs 1 and 2 are labeled as S_3 and U_3, respectively, and other candidate points are labeled as T_3 in the auxiliary plane [A3] as shown in Fig. 3(*h*). Next these points are projected back to auxiliary plane [A2]. If the edge view line is short, then it can be extended to meet the projection requirements (Ref. Fig. 3(*i*)). This means that the assumed edge view of the line drawn in step III (Fig. 3(*e*)) was short.

Step VII: Project the sinking points back to auxiliary plane [A1] in order to obtain S_1, U_1, and T_1. It can be seen in Fig. 3(*j*) that equal distances i, j, and k units from the reference line 2–3 are transferred to auxiliary plane [A1]. Similarly, the points are transferred to the bottom principal plane [B] by taking the distances n, l, and m from auxiliary plane [A2] as shown in Fig. 3(*k*) and the sinking points in the bottom plane (S_B, U_B, and T_B) are obtained.

Step VIII: Finally, the sinking points (U_B, S_B, T_B) are transferred to the frontal principal plane [F] by projecting the points from plane [A1] and taking the respective distance (r and s) from the reference line B-1 and then S_F, U_F, and T_F are obtained. It can be seen that the location of point S_F lies outside the boundary of the main skull and lies directly on the lower jaw. Therefore, this point can be ignored for the selection of sinking points as shown in Fig. 3(*l*). The required magnitude of deformation and direction can be achieved by using U as a sinking point and T as another sinking point. Both action units originating from point O must be activated to achieve the desired deformation. That is, $\overrightarrow{QU}$ must deform with a magnitude corresponding to R_1–R_2 and $\overrightarrow{OT}$ with an amount R_3–R_4.

4 Application of GFEAD Method to a Prototype Face

GFEAD method was implemented on a prototype face developed by using shape memory alloy as actuators. This section describes how the deformation and direction of movement can be analyzed by using GFEAD method. For a given configuration of sinking points and anchor points, the face deformation as a result of actuators being driven independently or in combination to each other was analyzed by considering representative configuration of anchor point–sinking points. The arrangements of actuators to activate the right cheek movement are shown Fig. 4. It consists of two sinking points A and B, anchor point O, and action units AU2 and AU2L. The action units AU2 and AU2L mimic the risorius

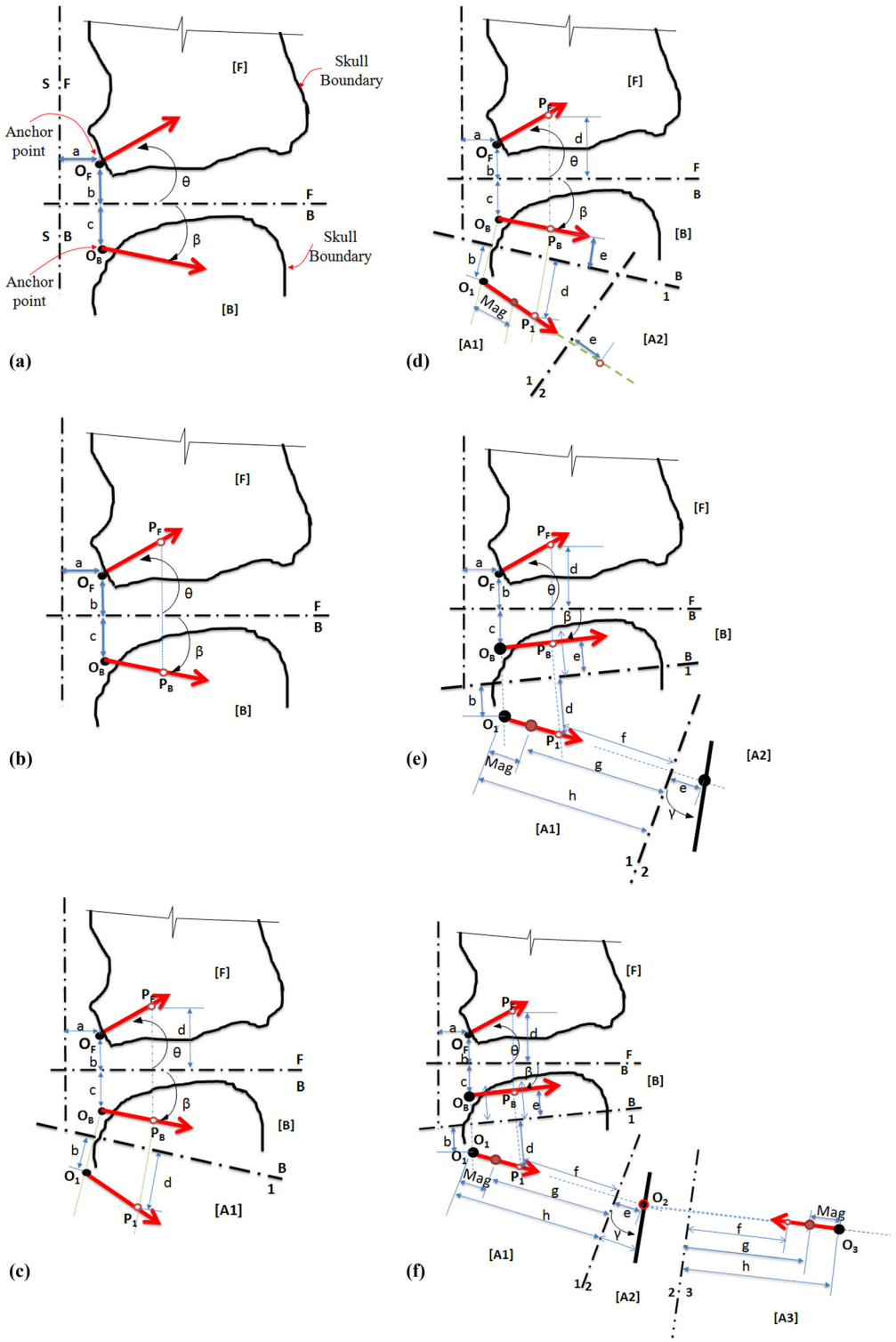

Fig. 3 Facial expression analysis and design in case II. (*a*) Schematic diagram of the desired direction of movement, anchor point, and boundary of the skull in two views. (*b*) *Step I*: Picking up any point on the directional line in the two principal planes (P_F and P_B). (*c*) *Step II*: An orthographic view showing the true length of deformation line (OP) in auxiliary plane [A1]. (*d*) *Step II:* Orthographic view that shows the point view of the facial deformation vector in auxiliary plane [A2] (*e*) *Step III*: Construction of an edge view of a plane that holds the sinking and the anchor points with an angle γ from reference line 1–2 in auxiliary plane [A2]. (*f*) *Step IV*: Construction of a parallel reference line 2–3 to the edge view line in order to obtain the true shape of the plane that holds the sinking points and the anchor point in plane [A3] (*g*) *Step V*: Construction of arcs with radius R_1 and R_2 centered at O_3 and Q_3, respectively, in auxiliary plane [A3] where R_1–R_2 corresponds to the displacement of the SMA actuator. Alternative circles are also drawn with radius R_3 and R_4 keeping the R_3–R_4 the same as the displacement of the SMA actuator. (*h*) *Step VI*: The candidate sinking points are the intersection of the arcs drawn in *step V* and marked as U_3, S_3, and T_3 in auxiliary plane [A3]. (*i*) *Step VI*: Projecting back the candidate sinking points to the edge view line in auxiliary plane [A2]. (*j*) *Step VII*: Projecting back the sinking points to auxiliary plane [A1] by mapping equal distance i, j, and k from plane [A3] to plane [A1]. (*k*) *Step VII*: Projecting the sinking points to the bottom principal plane [B] by transferring equal distance (l, m, n) from plane [A2].

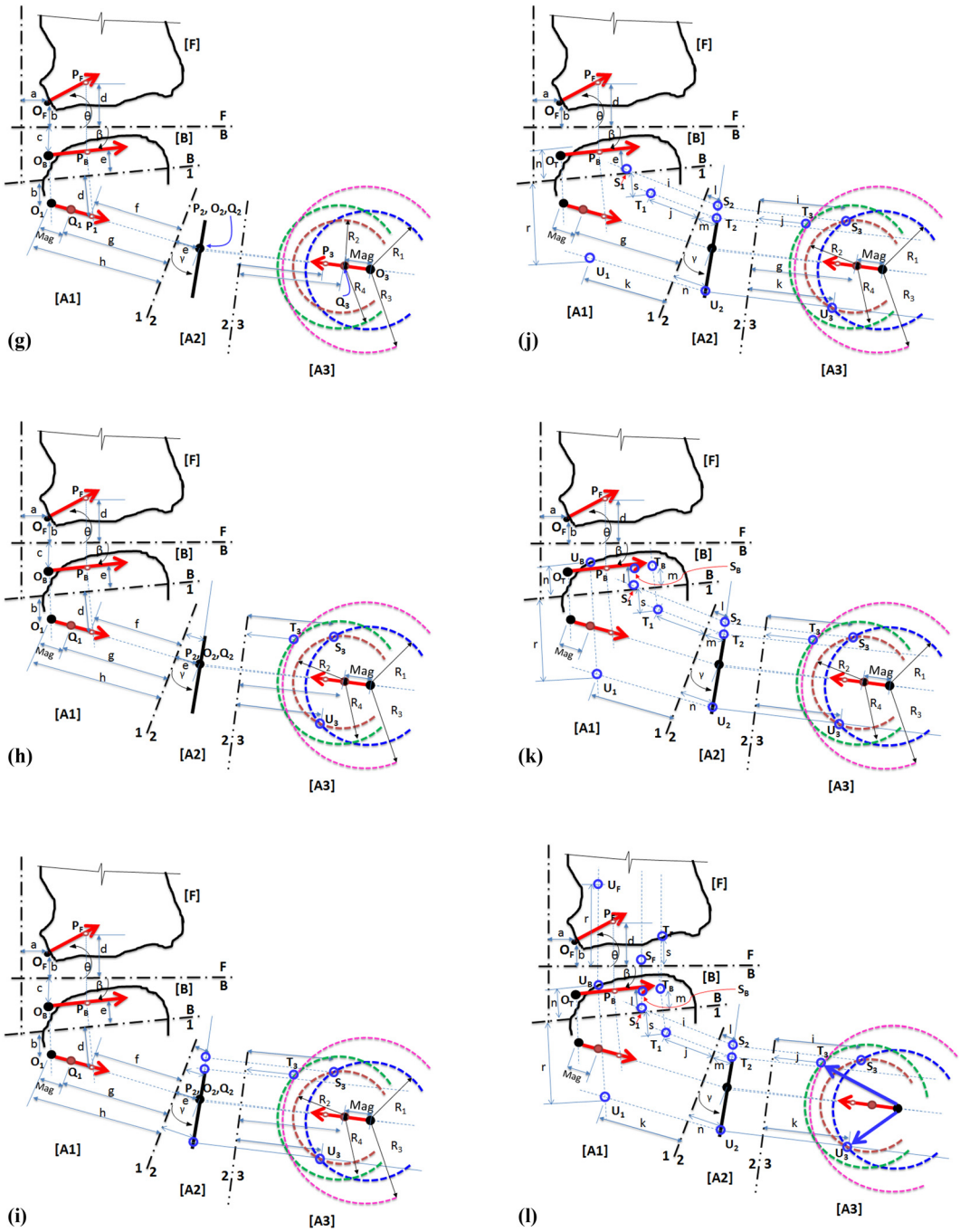

Fig. 3 (Continued).

and zygomaticus major muscle in human face. The corresponding distances from reference plane are also shown in the figure. Following the procedure described in case I and referring to Fig. 4, the auxiliary plane that provides us the actual deformation of action units can be obtained as shown in auxiliary plane [A3]. In the plane [A3], three cases are analyzed as follows: (1) when the lower action unit AU2L (line OB) is activated, (2) the upper action unit AU2 (Line OA) is activated independently, and (3) when both are simultaneously actuated. All the three cases are shown in each plane with indices and after projecting back to the frontal view of interest, the total apparent deformation can be obtained. The following assumptions are made in the analysis: (i) SMA generates maximum strain, (ii) there is no friction between the SMA and underlying skull, and (iii) the origin of the action unit is estimated accurately. Considering the actuator length at the action unit AU2 and AU2L (265 mm) and 4% strain, different cases can be studied. A detailed view of the deformation direction and magnitude is shown in the inset of Fig. 4(*b*). On the frontal plane ([F]) of this figure, it can be seen that: (1) actuating the upper action unit provides a 10 mm deformation directed towards the sinking point A_F (86 deg with respect to the horizontal line), (2) if the lower action unit is activated with 4% strain, the deformation in the front will appear as 8 mm projected toward the sinking point with 19 deg angle, and (3) in the case where both actuators are activated, the magnitude is amplified as 14 mm with 60 deg angle. The length of the actuator was taken to be 265 mm for both action unit AU2 and AU2L. The deformation magnitude and direction computed here are the theoretical values when elastomeric skin was not mounted on the skull. To account for the effect of skin elasticity, the thickness of the skin, and the

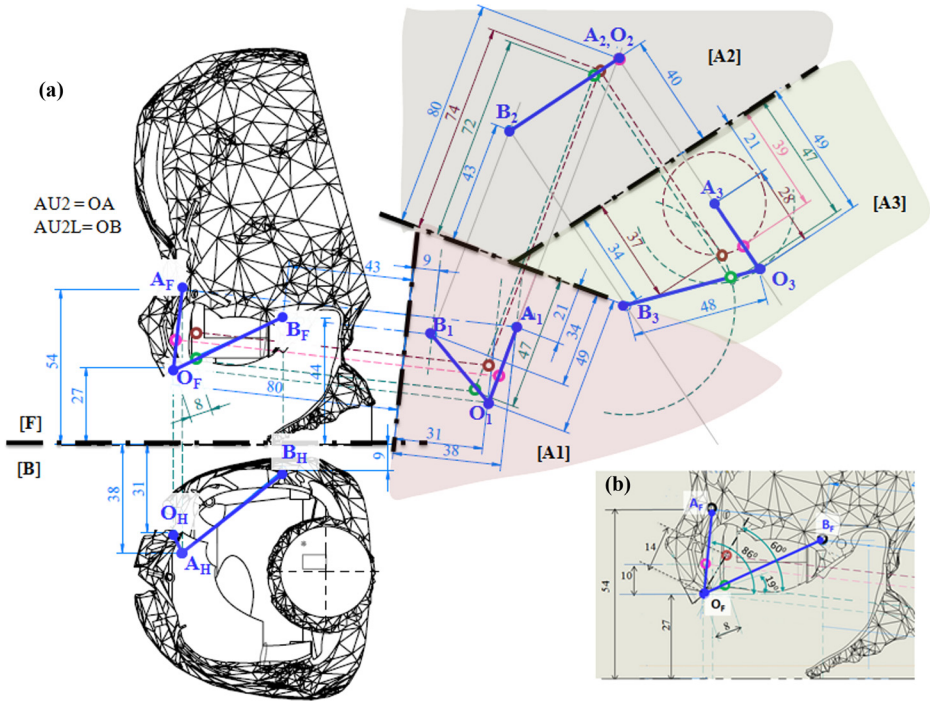

Fig. 4 (*a*) Analysis of facial expression on a prototype skull focusing on the right cheek movement. (*b*) Inset view of the front skull indicating three cases of positions and directions of control points (pink, maroon and green hollow circles).

mounting configuration of actuators, the deformation can be predicted by taking efficiency of deformation as a variable. The direction of deformation will be same with the skin and without the skin as long as the origin and the sinking points are determined to a reasonable accuracy in the analysis.

Sometimes the control point (anchor point) may not be determined accurately since they are embedded in the skin and mounted on the skull assembly. In that case, GFEAD method can be used to study the variation in the vicinity of the estimated action unit origin. Prototypic facial expression is often displayed by a number of discrete actuators rather than a continuous sheet of skeletal facial muscles and fibers in biological systems. Therefore, different configuration of actuator arrangement can be encountered during the design phase of prototypic face. We illustrate here a typical example of arrangement of sinking points and action unit as shown in Fig. 5. In this case, an interesting phenomenon can be observed when one of the actuator demonstrates a slacking effect rather than rotation. The arrangement of sinking

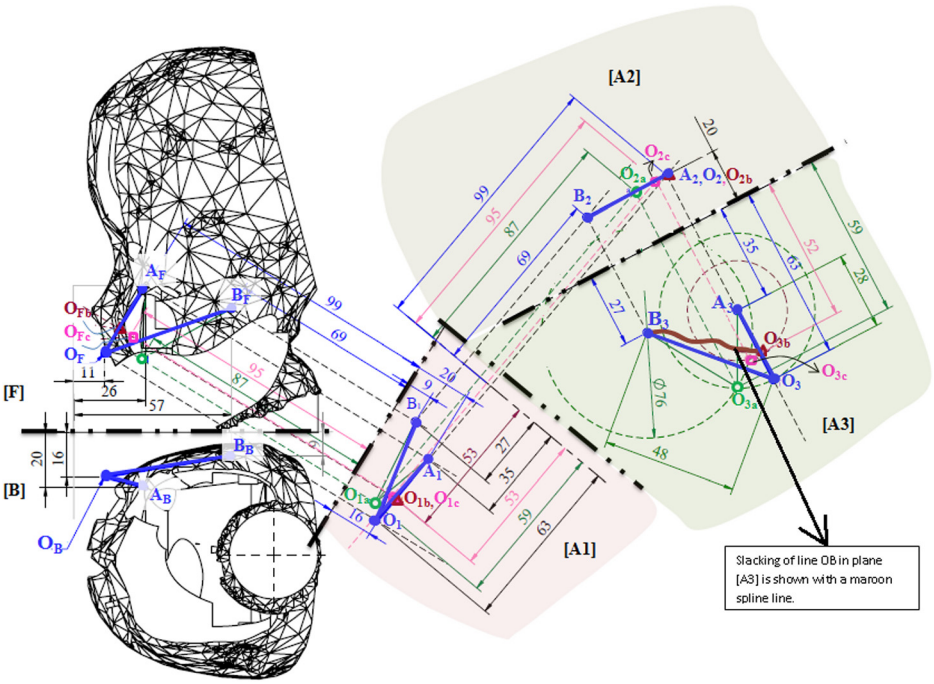

Fig. 5 Illustration of the slacking phenomena

point and action unit are labeled in the frontal and bottom view of the skull coordinate system as shown in Fig. 5. After projecting the points in the auxiliary plane that provides the real deformation in plane [A3], the slacking phenomena will occur in one of the actuators. This implies that the given arrangement of sinking points and action unit allows one actuator to lose its tensile stress. This happens when the actuator shown in A_3O_3 deforms 4% while B_3O_3 is not activated. Note that the illustration shown in Fig. 5 is practical values measured from the prototypic face considering different control points attached to the skin. Details of the procedure are shown in Fig. 5 following similar procedure as described in previous sections. The slacking phenomenon is one of the advantages of using the GFEAD method because this behavior cannot be easily observed with analytical solution or any other methods. In addition, this method will provide information related to interference to the mechanical system (cables and pulley systems).

5 Prototype Face Characterization From Video Imaging and Model Verification

The face deformation can be accurately characterized by either taking a video parallel to the surface of deformation or two orthogonal sets of images. In our case, measurements on a prototype baby face were done by a digital camera aligned parallel to the surface of motion after the skin has been assembled. The smiling expression was considered for representative analysis focusing on the mouth area. The control point near to the edge of the mouth was connected to the action units AU2 and AU2L. Both action units can be activated separately or independently to control the direction of motion and magnitude of deformation. The direction of movement and magnitude were determined by tracking a circular disc which was glued to the edge of the lips. Three cases shown in Fig. 6 demonstrate the magnitude of deformation and direction of movement. In Fig. 6(*a*), when the upper SMA wire was activated (sinking point indicated as a hollow triangular mark), the anchor point moved 3.5 mm toward the sinking point with 66 deg angle from the horizontal. The corresponding directional vector on the prototype face is shown in a magnified view in Fig. 6(*b*). In the case where only the lower SMA wire was activated, a 5 mm facial deformation having 4 deg angle with respect to the horizontal plane was observed. The angle was directed toward the sinking point of SMA2 (AU2L). Figures 6(*c*) and 6(*d*) illustrate the facial movement and direction of the motion vector, respectively. In the third case, where both SMA actuators were activated, an 8 mm deformation having 10 deg angle with respect to horizontal plane was measured. The direction of movement was in between the two extreme cases. The small displacement is due to the fact that a baby humanoid head was utilized ($140 \times 110 \times 90$ mm^3) in the experiments with a number of pulleys and SMA actuators that have limited displacement. The deformation on the face can be clearly seen from the video sequences since the whole surface around the cheek moves with some wrinkles. Therefore, the magnified views of the edge of the mouth are shown on the right side of Fig. 6. All image processing was done in MATLAB Image Processing Toolbox. The configuration of control points and sinking points was close to that predicted by the analysis presented in Fig. 4. Comparing the deformation measured on the elastomeric skin and the magnitude determined by the graphical method shown in Fig. 4, the experimental values were less. This can be attributed to the inconsistency in allocating holes from CAD to prototyping, the friction between the skull surface and the skin, attachment point's performance, elasticity of the skin, and also alignment of the camera during measurement. These values can be accounted by computing the efficiency of deformation transfer. The efficiency of deformation which is defined as the ratio of experimental to theoretical deformation can be obtained for the graphical method. In this case, without considering skin properties the efficiencies are $\eta_{Au2} = 35\%$, $\eta_{Au2L} = 62\%$, and $\eta_{Au2L\ \&\ AU2} = 57\%$. The efficiency of deformation angle without considering skin properties are: $\eta_{Au2} = 76\%$, $\eta_{Au2L} = 21\%$, and $\eta_{Au2L\ \&\ AU2} = 17\%$.

6 Discussion on the Effect of Skin Properties, Friction, and Curved Geometries

In this section, we discuss on uncertainty that could arise in the GFEAD method. The dominant uncertainty that could arise using this method is related to skin properties (such as skin material, stiffness, and thickness), friction between the skull and the skin, and the attachment points on the skin.

6.1 Skin Properties. The skin properties affect the overall movement of anchor points depending on the thickness, the material used, and the elasticity. These properties can be compensated by choosing appropriate number of actuators attached at a particular point. The skin thickness map of the robotic head was taken by piercing the skin with pins at various locations and taking the measurements on depth of penetration. The overall thickness map was determined by normalizing with the lowest skin thickness point which happens to be around the nose (2.33 mm). The normalized thickness map of the face is shown in Fig. 7(*a*). It can be seen that the thickness of skin was not uniform over the entire facial structure indicating the difficulty in analyzing the problem. The force–displacement relationships of the robotic head were measured with a force sensor. To illustrate the deformation of skin along with the force requirement, let us consider the lower left side of the cheek as shown in Fig. 7(*a*), indicated by a dotted line. Schematic diagram of the interconnection at points O, A, and B are illustrated in Fig. 7(*b*) with equivalent skin stiffness indicated by K_1 and K_2. These values can be measured experimentally and detailed measurement technique can be found in Ref. [4]. These stiffness values are the effective spring constant that contribute toward the deformation of the skin ($K_1 = 0.135$ N/mm and $K_2 = 0.074$ N/m).

6.2 Friction. The attachment configuration between the skin and the skull affects the overall movement and force required to pull the skin. It was shown earlier in Fig. 1(*a*) that the skull geometry has open areas that do not contact with the skin. In those sections, there will be no friction between the skull and the skin during actuation. In other areas like the frontal head, the skin slides over the surface of the skull. Three cases of friction in a skull–skin interaction are presented in Figs. 7(*c*)–7(*e*): (i) friction encountered along the edge (shown in Fig. 7(*c*)), (ii) friction is partially present between skin and skull (Fig. 7(*d*)), and (iii) friction is present on the entire surface between skin and skull (Fig. 7(*e*)). The cut-out portion of the skin can be observed in its actual size in a normal plane (the plane that contains A_3, B_3, and O_3 in Fig. 4). On that plane, the deformation of skin can be analyzed by accounting for skin properties and friction. To overcome the friction, the force of actuator can be increased for instance by increasing the number of actuators that originate at a particular point. For example, in the current prototype, the number of actuators that originate from point O and terminate at points A and B is two. This increases the force required to push the skin in the desired direction and hence overcomes the friction resistance. The important aspect of GFEAD method is that it provides the actual deformation in the auxiliary plane that has all the sinking and origin points in their exact shape. In that case, static and dynamic equations can be employed to further analyze the deformation on that plane and propagate back to the frontal plane. If the system is represented by spring–mass–damper system, the governing dynamic equations will be

$$-f + F = m_{eq}\ddot{x} + c_{eq}\dot{x} + K_{eq}x = F_{eq} \tag{1}$$

In the steady state, considering only static deformation, $\ddot{x}$ and $\dot{x} = 0$, the equations reduce to

$$K_{eq}x = F_{eq} = -f + F \tag{2}$$

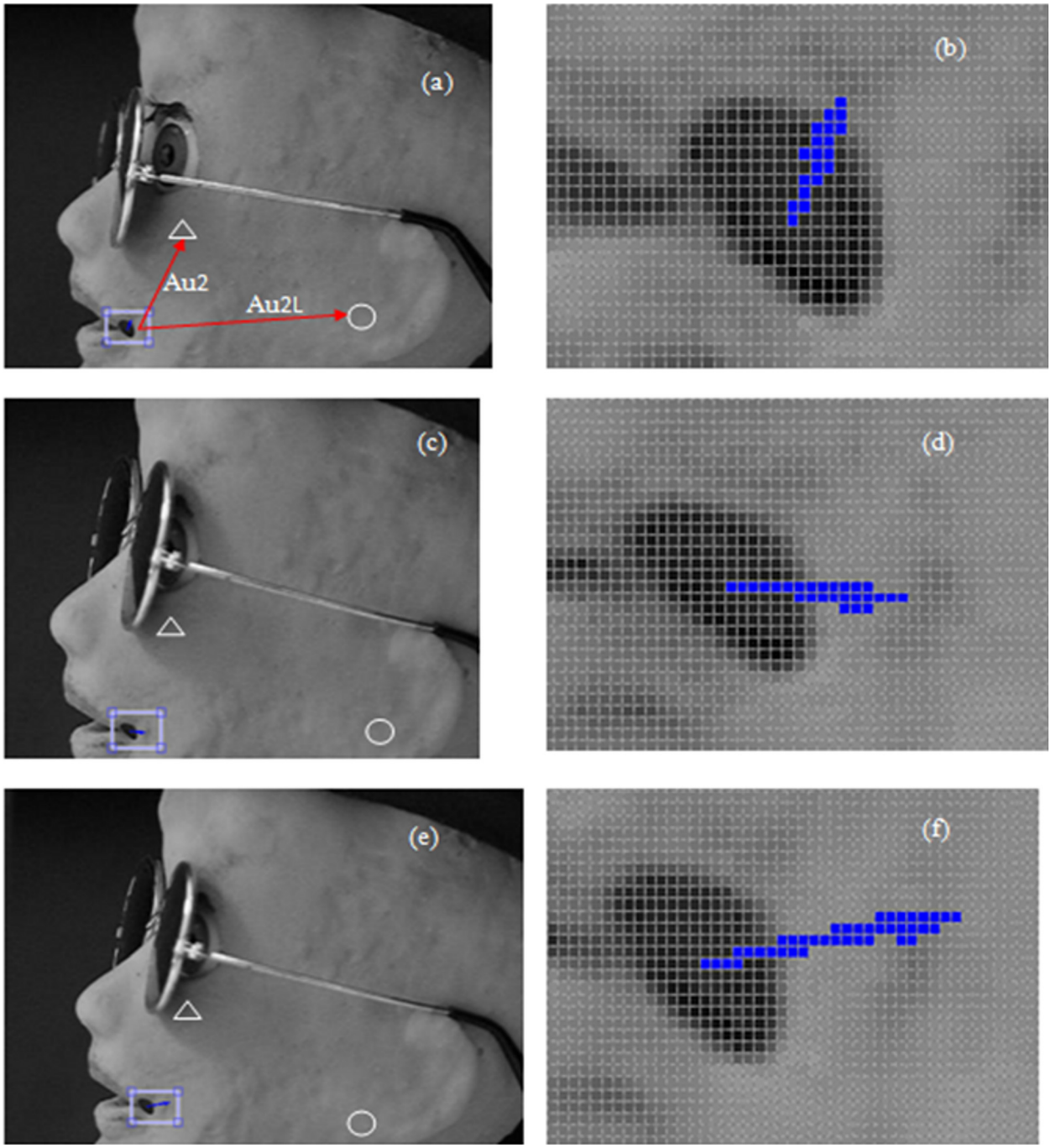

Fig. 6 Three different facial deformations on a prototype face, (*a*) and (*b*) upper SMA activated by 3.5 mm, (*c*) and (*d*) action unit AU2 activated resulting in 5 mm deformation, (*e*) and (*f*) both upper and lower SMA activated by 8 mm

where F is the force applied by the SMA actuator (contractile actuator), f is the friction force, K_{eq} is the equivalent local spring stiffness of the skin, and x is the deformation of the skin. One can easily see that the deformation magnitude which is dependent on the friction can be compensated by increasing the number of SMA actuators used at the anchor point.

6.3 Compensation for Friction and Skin Properties. The effect of skin properties and friction on the deformation of the skin can be compensated by focusing on the number of actuators. For multiple number of contractile actuators connected at a particular action unit, the determination of operating points can be done by analyzing the load line and actuator characteristics, and assuming that the actuator has a linear profile of stress–strain (force–displacement). Considering Fig. 8, for one SMA actuator with blocking force F_b and practical free strain ε_f, the relationship can be expressed by a linear line with negative slope. If two SMA actuators of the same length are used together in parallel, the force will be amplified by two times. Therefore, force gets amplified by the number of SMAs attached at a particular point. The skin characteristic curve is a positive slope line. The action unit can be connected to a number of shape memory alloy actuators with each action unit having its own unique displacement characteristics because the thickness of skin at each action unit is different resulting in force anisotropy. Therefore, it is relevant to study the force and displacement relationship rather than stress–strain relationship. Figure 8 demonstrates the shape memory actuator

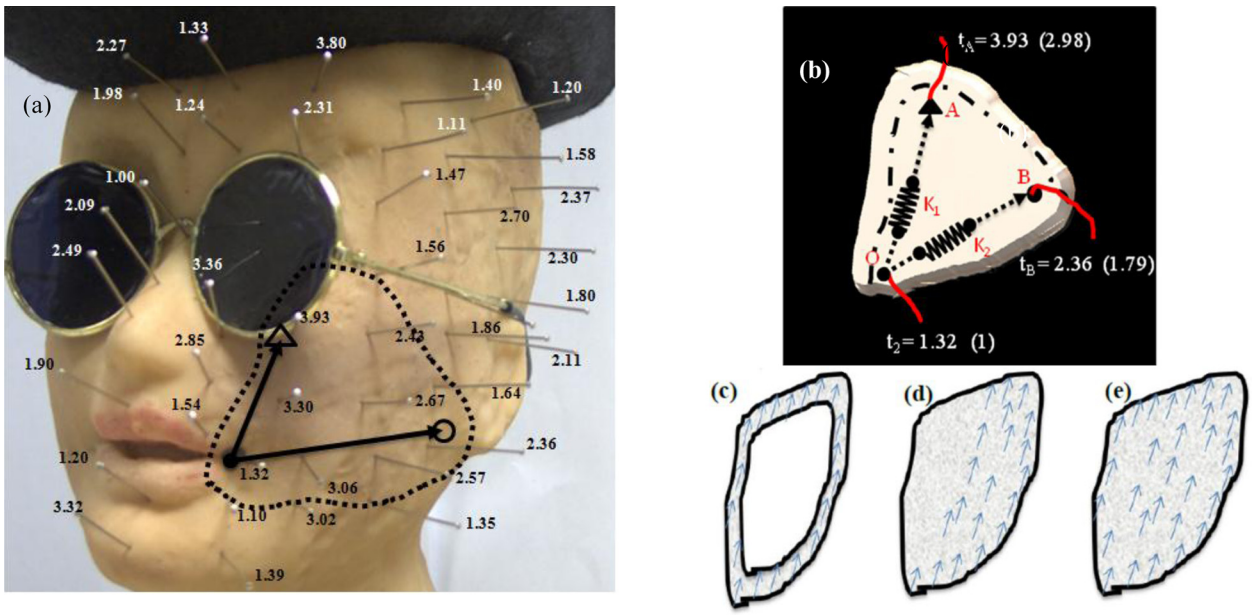

Fig. 7 (*a*) Thickness-map of the baby face and left portion of the skin–skull assembly and contact between the skull and the skin, (*b*) schematic diagram of the inset of skin around the cheek, (*c*) friction contact only on the periphery, (*d*) supporting skull is partially touching the skin, and (*e*) supporting skull and skin contacts on the entire surface

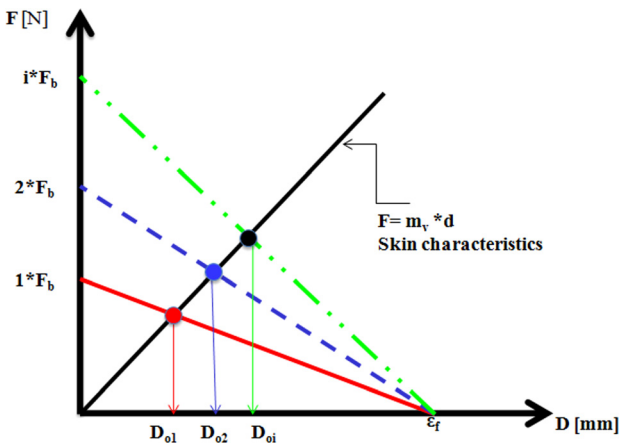

Fig. 8 Effect of number of actuators and skin properties on the movement of control points

force–displacement characteristics. The governing equation for multiple SMA actuators connected at an action unit can be considered as a linear line

$$F = iF_b\left(\frac{-D}{\varepsilon_f} + 1\right) \tag{3}$$

where F is actuator force, F_b is the blocking force of SMA, i is the number of actuators with same diameter, D is the magnitude of displacement, and ε_f is the displacement due to free strain. The load line could be a variable across the face of the robot and it can be determined experimentally. This relationship can be represented as

$$F = m_v D \tag{4}$$

where F is the force required to stretch the skin, m_v is the slope of the skin characteristic (determined experimentally), and D is the displacement. The operating point of the action unit on the face can be determined by the intersection of Eqs. (3) and (4) given as

$$D_{oi} = (iF_b)\left(\frac{iF_b}{\varepsilon_f} + m_v\right)^{-1} \tag{5}$$

Equation (5) depicts how the operating point, which is the point of interest, is displacing under different configuration of SMA arrangement. For the case near the cheek, the skin properties and friction encountered can be measured experimentally. These values were found to be: $m_v = 0.135$ and 0.074 N/mm for AU2 and AU2L, respectively. The number of actuators attached to both action units was two. The blocking force of Biometal fiber actuators was 3.9 N (500 MPa). The operating point of action unit considering skin properties and interaction with the skin can be obtained from Eq. (5) as $D_{oi} = 8.95$ and 9.63 mm. This deformation refers to the actual one in auxiliary plane [A3] in Fig. 9. After reprojecting the operating points toward the frontal plane, the deformation magnitude can be obtained. A magnified view of the direction and deformation are shown in Fig. 9(*b*). If only AU2 is actuated, a displacement of 9 mm directed 77 deg with respect to the horizontal line is achieved; if only AU2L is actuated, then 10 mm deflection directed 19 deg with respect to the horizontal line is observed; and if both are actuated, then 11 mm deformation directed 59 deg with respect to the horizontal line is obtained.

The efficiency of deformation magnitude for this method considering skin properties were $\eta_{Au2} = 38\%$, $\eta_{Au2L} = 50\%$, and $\eta_{Au2L\ \&\ AU2} = 72\%$. The efficiency of deformation angle for this method without considering skin properties were $\eta_{Au2} = 85\%$, $\eta_{Au2L} = 21\%$, and $\eta_{Au2L\ \&\ AU2} = 17\%$. The error was due to the slight difference in allocation of the origin of the action unit in the CAD model and the experimentally characterized face. Therefore, a precise allocation of action unit after the skin is mounted on the skull is required to achieve a perfect analysis tool. This issue is beyond the scope of this paper and will be addressed in the future. Note that the graphical method presented here assumes that the location of the origin of the action unit is known. Based on these results, we believe that the approach presented here will be an excellent asset for humanoid facial expression research.

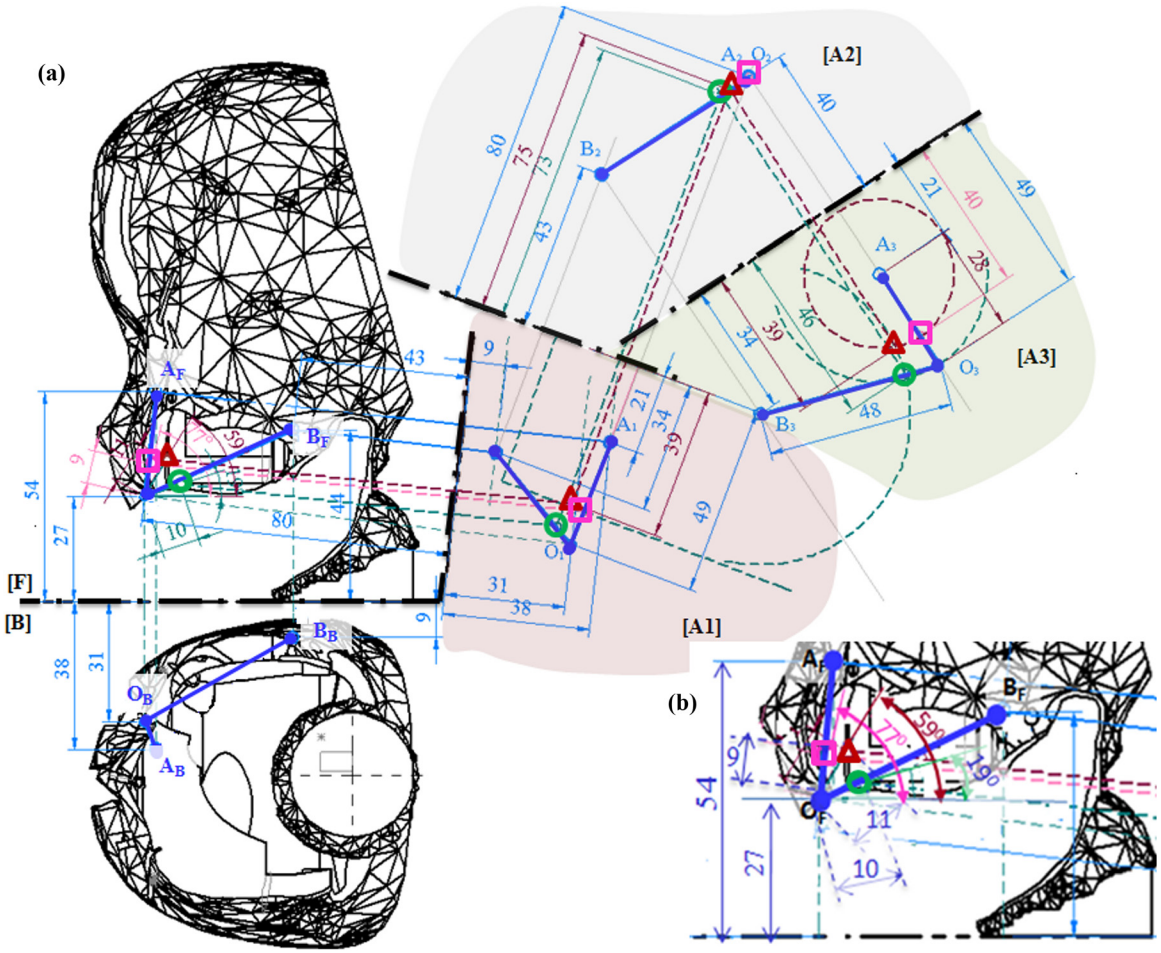

Fig. 9 (*a*) GFEAD considering skin elasticity and number of actuators, (*b*) Zoomed view of the frontal plane considering skin properties

The graphical method presented here can be used for routine analysis because one can easily change the location of the sinking point in the normal plane that shows the entire action unit and sinking point and propagate back to the frontal plane. Therefore, the location of sinking point can be easily changed and their effect can be seen quickly in the frontal plane.

6.4 Discretization for Curved Geometry. For the case, where anchor point and sinking points do not lie on same plane, the graphical analysis can be done by discretizing the curved plane. For example, in the case presented in Fig. 7(*a*), had the skull geometry been fully solid, then the skin would slide over the curved surface. Also, the sinking points A and B and the origin O would lie in a curved plane. In such case, discretization can be made by choosing a climax point on the curve. Consider two views of a cut-out of a curved skull as shown in Fig. 10(*a*). The front view in this figure shows anchor point O and sinking points A and B. On the left side, lines OA and OB lie on the curved plane. In such case, peak points on the curve such as points C and D should be taken to form two planes OCD and CABD. Figure 10(*b*) depicts the choice of points C and D and the formation of the planes. Following the procedure as described in case II of the analysis, the planes can be projected to auxiliary views. Note that the analysis considers a contractile actuator. For SMA actuators and ABS plastic skull, the description on curved plane is not useful because if SMA actuator slides over a plastic, the plastic melts the skull structure as the temperature of SMA reaches 90 °C. However, if the SMA is embedded within the elastomeric skin,

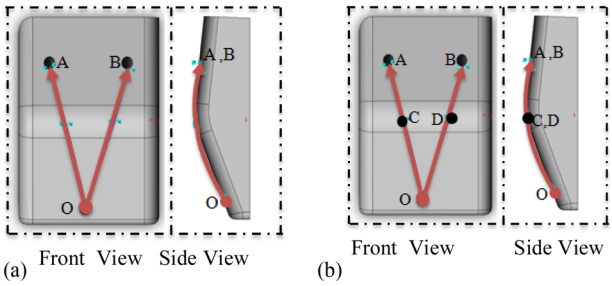

Fig. 10 (*a*) Arrangement of action unit and sinking points on a curved plane. (*b*) Discretization of action unit and sinking points on a curved plane.

the analysis still holds. For other actuation technologies utilizing wire based system, the description is directly applicable.

6.5 Full Face Characterization. The facial emotion of a robotic head is a result of deformation of soft elastomeric skin due to actuation of a single action unit or a combination of action units. The facial expressions from the current prototype face robot are demonstrated in Fig. 11. To help in realizing the generated emotion, the schematic diagram of the AUs is depicted in Fig. 11(*a*) where 11 AUs are shown pulling the control points (anchor points) towards the sinking points. Multiple facial emotions from the prototype robot face are presented to illustrate the capability in small scale robot head. Figure 11(*b*) is the normal appearance

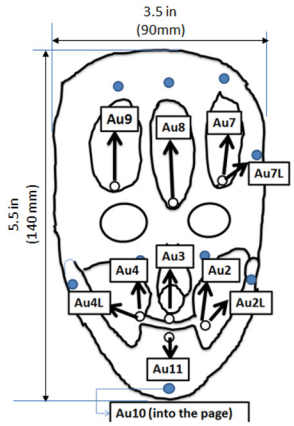

(a). Action units(AUs) on the skull

(b). Normal face

(c). AU2L(Risorius), left cheek stretched (smirk)

(d). AU3(Philtrum), upper lip up (sneer action)

(e). AU8(Procerus), both brow raised (concerned)

(f). AU10(Lateral pterygoid + digastric) , mandible pulled down(mouth opened)

(g) AU9 (Outer Frontalis), right eye brow lift up (mischievous/ nervous)

(h) AU10 + AU2L, left check and mandible opened ("eh")

(i). AU8 stretched, (worried)

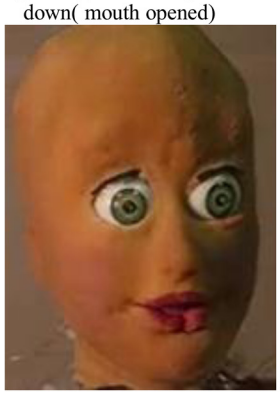

(j). AU11+AU8, surprised and angry

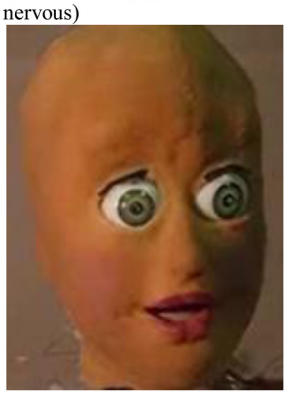

(k) AU10 shocked

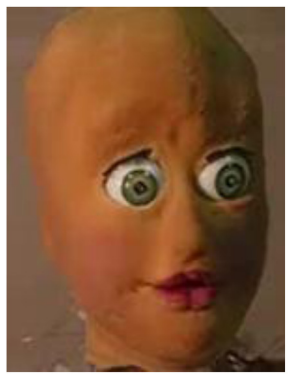

(l) AU3 + AU11 "uhh"

The expression (i)-(l) are when the upper head is stretched (AU9 and AU7 stretched)

Fig. 11 Various facial emotions from the prototype face developed using shape memory alloy actuators. The size of the skull is 140 × 90 × 110 mm^3. (*a*) AUs on the skull, (*b*) normal face, (*c*) AU2L (risorius), left cheek stretched (smirk), (*d*) AU3 (philtrum), upper lip up (sneer action), (*e*) AU8 (procerus), both brow raised (concerned), (*f*) AU10 (lateral pterygoid + digastric), mandible pulled down (mouth opened), (*g*) AU9 (outer frontalis), right eye brow lift up (mischievous/ nervous), (*h*) AU10 + AU2L, left check and mandible opened ("eh"), (*i*) AU8 stretched (worried), (*j*) AU11 + AU8, surprised and angry, (k) AU10 shocked, (*l*) AU3 + AU11 "uhh." The expressions (*i*)–(*l*) are when the upper head is stretched (AU9 and AU7 stretched).

of the face and Fig. 11(*c*) is when the left cheek is stretched by the action unit AU2L. This action unit is often called risorius muscle. Since one of the cheek muscles is activated, it can be considered as smirk. Figure 11(*d*) shows the raised upper lip. In other words, lifting the ridge of the lips (philtrum) and exhibiting sneer kind of emotion. Figure 11(*e*) is the action caused by the AU8 which lifts up both eye brows and makes a concerned/surprise emotion. The action unit AU8 has similar function as procerus muscle in human face. Figure 11(*f*) is another class of surprise emotion with wide opening of the lower mandible using the action unit AU10. Figure 11(*g*) is the outer frontalis movement that raises the right eye brow using action unit AU9. Figure 11(*h*) is a combination of AU10 and AU2L which sounds like "eh" expression on the robotic face. Figure 11(*i*)–11(*l*) are a class of surprise, worried,

and shocking facial expressions, which typically are characterized by wide opening of the eyes with AU7 and AU9. If the skin is tightly attached with the skull during assembly, the face will show surprised emotion because this will create a tension on the AU7 and AU9. When the mouth area is actuated, the combination will produce different kind of facial expression. For example, in Fig. 11(*i*) a worried face can be seen by actuating AU8. In Fig. 11(*j*), an angry and surprised face is seen by activating AU11. A shocking emotion is illustrated by triggering AU10 and letting the mouth open wide. Finally, an "uhh" kind of expression is obtained by invoking the AU3. The facial emotions demonstrated in Fig. 11 are some class of expression obtained from the prototype and the effect is usually dependent on the length of wire, the spacing inside the skull, the attachment points, and the anchor points. The GFEAD in this case will be useful to allocate the location of sinking points and to optimize the space by finding the best arrangement of actuators. The GFEAD method has been implemented on the left cheek so that one can analyze the configuration of actuators and their effect on the deformation behavior. Obviously, the emotions demonstrated are typically dependant on the magnitude of deformation, the location of sinking points, the attachment points, and the skull geometry. These parameters are essentially dependant on the size of the robotic head. Especially, for small scale baby humanoid robot, space limitation is the major factor. Therefore, a precise method of designing and analyzing the deformation is absolutely required.

7 Significance of GFEAD Method

(1) The significance of graphically solving the parameters for facial expressive humanoid prototype (location of terminating points or sinking points; deformation amplification with different configuration of attachment points, and directional control of movement) can be easily visualized in two-dimensional surface.
(2) FACS established in 1978 provides us 44 action units responsible for facial expression in human. However, the replication of FACS on humanoid prototypes has been limited due to space constraints, absence of suitable actuator technologies, and limited computational and analysis techniques. GFEAD overcomes one of the challenges related to design process by providing the method for determining the arrangement of actuators along with their resulting deformation. Currently, the most advanced human-sized head has 31 DOF facial and neck motion [9,41].
(3) The operations involved in the analysis are simple such as mapping positions from auxiliary plane or inscribing a circle of known radius. Thus, this method can be adopted for routine analysis which is essential in the design of intricate geometry since the positions of sinking points can be changed easily.
(4) GFEAD describes or reveals singular points or complex configuration of muscle–skin arrangement used in the design process. Any magnitude of deformation assumed in the initial stage can be cross-checked.
(5) Three-dimensional models are often difficult to work with and require high speed computation. This method, however, uses only two-dimensional planes to analyze facial expression and thus it does not need much computational power.
(6) GFEAD method can be easily modified for supporting skull structure with action unit and terminating point's falling on curved geometry by discretizing the curved plane with triangles.
(7) GFEAD significantly reduces mathematical error as it does not require the explicit mathematical representation of vector space and different configuration of action unit arrangement.
(8) It reveals important manifestation of slacking phenomena that would be difficult to observe with other techniques and create interference with mechanical systems.
(9) In general, the benefit of this work is that it will provide designer a means of allocating the sinking points in order to obtain a desired magnitude and direction of deformation or analyze the deformation behavior for a given configuration of anchor point-sinking point arrangements.

8 Summary

Creating human-like expression comprising artificial muscles, elastomeric skin, and mechanical components requires a computational tool to analyze the architecture of prototype. In this paper, we have presented a method for determining the sinking points that controls the direction of facial movement and analyzes the configuration of actuators by utilizing only two-dimensional orthographic planes. The control points at the action units are assumed to be known beforehand. We considered two cases for the demonstration of the method—case I: Determination of direction of movement and magnitude for a given configuration, and case II: Given only desired direction and magnitude of movement on a prototype face, determining the sinking points of the contractile actuator. The proposed analysis and design tool was implemented on a CAD design of a prototypic robotic face and encouraging results were obtained within the limit imposed by the error in estimation of action units in the CAD design and elasticity of skin.

Acknowledgment

This research is financially supported by the Institute for Critical Technology and Applied Science, Virginia Tech, and Office of Naval Research through MURI program.

References

[1] Tadesse, Y., Bergs, R., Priya, S., Stephanou, H., Popa, D., and Hanson, D., 2006, "Piezoelectric Actuation and Sensing for Facial Robotics," Ferroelectrics, **345**, pp. 13–25.
[2] Tadesse, Y., and Priya, S., 2009, "Humanoid Face Utilizing Rotary Actuator and Piezoelectric Sensor," Paper No. IMECE2008-66860.
[3] Tadesse, Y., Subbarao, K., and Priya, S., 2010, "Realizing a Humanoid Neck With a Four Bar Mechanism," J. Intell. Mater. Syst., **21**(12), pp. 1169–1191.
[4] Tadesse, Y., Hong, D., and Priya, S., 2011, "Twelve Degree of Freedom Baby Humanoid Head Using Shape Memory Alloy Actuators," ASME J Mech. Rob., **3**(1), pp. 1–18.
[5] Tadesse, Y., Priya, S., Chenthamarakshan, C. R., de Tacconi, N. R., and Rajeshwar, K., 2008, "Polypyrrole-Polyvinylidene Difluoride Composite Stripe and Zigzag Actuators for Use in Facial Robotics," Smart Mater. Struct., **17**(2), p. 025001.
[6] Tadesse, Y., Grange, R. W., and Priya, S., 2009, "Synthesis and Cyclic Force Characterization of Helical Polypyrrole Actuators for Artificial Facial Muscles," Smart Mater. Struct., **18**, p. 085008.
[7] Berselli, G., Vertechy, R., and Castelli, V. P., 2009, "Design of a Single-Acting Constant-Force Actuator Based on Dielectric Elastomers," ASME J. Mech. Rob., **1**, p. 031007.
[8] Papadogiorgaki, M., Grammalidis, N., Makris, L., and Strintzis, M. G., 2006, "Gesture Synthesis From Sign Language Notation Using MPEG-4 Humanoid Animation Parameters and Inverse Kinematics," *Proceedings of the 2nd IET International Conference on Intelligent Environments*, pp. 151–160.
[9] Oh, J. H., Hanson, D., Kim, W. S., Han, Y., Kim, J. Y., and Park, I. W., 2006, "Design of Android Type Humanoid Robot Albert HUBO," *Proceedings of the International Conference on Intelligent Robots and Systems,* IEEE/RSJ, pp. 1428–1433.
[10] Kim, D. H., An, K. H., Ryu, Y. G., and Chung, M. J., 2007, "A Facial Expression Imitation System for the Primitive of Intuitive Human-Robot Interaction," *Human-Robot Interaction*, N. Sarkar, ed., Itech Education and Publishing, Vienna, Austria, p. 522.
[11] Hashimoto, T., Hitramatsu, S., Tsuji, T., and Kobayashi, H., 2006, "Development of the Face Robot SAYA for Rich Facial Expressions," *SICE-ICASE International Joint Conference*, pp. 5423–5428.
[12] Shimada, M., Minato, T., Itakura, S., and Ishiguro, H., 2006, "Evaluation of Android Using Unconscious Recognition," *Proceedings of the 6th IEEE-RAS International Conference on Humanoid Robots*, pp. 157–162.
[13] Mavridis, N., and Hanson, D., 2009, "The IbnSina Center: An Augmented Reality Theater With Intelligent Robotic and Virtual Characters," *Proceedings of IEEE International Symposium on Robot and Human Interactive Communication*, pp. 681–686.
[14] Hanson, D., Baurmann, S., Riccio, T., Margolin, R., Dockins, T., Tavares, M., and Carpenter, K., 2008, "Zeno: A Cognitive Character," *AAAI Workshop*, Technical Report No. WS-08-08, pp. 9–11.

[15] Kanade, T., Cohn, J. F., and Tian, Y., 2000, "Comprehensive Database for Facial Expression Analysis," *Proceedings of the 4th IEEE International Conference on Automatic Face and Gesture Recognition*, pp. 46–53.
[16] Ekman, P., and Friesen, W. V., 1978, *Facial Action Coding System*, Consulting Psychologist Press, Palo Alto, CA.
[17] Tian, Y., Kanade, T., and Cohn, J. F., 2001, "Recognizing Action Units for Facial Expression Analysis," IEEE Trans. Pattern Anal. Mach. Intell., **23**(2), pp. 97–115.
[18] Pei, X., Yu, J., Zong, G., Bi, S., and Hu, Y., 2009, "A Novel Family of Leaf-Type Compliant Joints: Combination of Two Isosceles-Trapezoidal Flexural Pivots," ASME J. Mech. Rob., **1**, p. 021005.
[19] Lavagetto, F., Pandzic, I. S., Kalra, F., and Thalmann, N. M., 1996, "Synthetic and Hybrid Imaging in the HUMANOID and VIDAS projects," *Proceedings of the International Conference on Image Processing*, Vol. 3, pp. 663–666.
[20] Chaminade, T., Franklin, D., Oztop, E., and Cheng, G., 2005, "Motor Interference Between Humans and Humanoid Robots: Effect of Biological and Artificial Motion," *Proceedings of the 4th International Conference on Development and Learning*, pp. 96–101.
[21] Kikuchi, M., Ogino, M., and Asada, M., 2004, "Visuo-Motor Learning for Behavior Generation of Humanoids," *Proceedings of the 2004 IEEE/RSJ International Conference on Intelligent Robots and Systems*, Vol. 1, pp. 521–526.
[22] Laschi, C., Miwa, H., Takanishi, A., Guglielmelli, E., and Dario, P., 2003, "Visuo-Motor Coordination of a Humanoid Robot Head With Human-Like Vision in Face Tracking," *Proceedings of ICRA '03, IEEE International Conference on Robotics and Automation*, Vol. 1, pp. 232–237.
[23] Lee, H. S., Park, J. W., and Chung, M. J., 2006, "An Affect-Expression Space Model of the Face in a Mascot-Type Robot," *Proceedings of the 6th IEEE-RAS International Conference on Humanoid Robots*, pp. 412–417.
[24] Lee, H. S., Park, J. W., and Chung, M. J., 2007, "A Linear Affect-Expression Space Model and Control Points for Mascot-Type Facial Robots," *IEEE Trans. Rob.*, **23**(5), pp. 863–873.
[25] Hasanuzzaman, M., Zhang, T., Ampornaramveth, V., Gotoda, H., Shirai, Y., and Ueno, H., 2005, "Knowledge-Based Person-Centric Human-Robot Interaction Using Facial and Hand Gestures," *Proceedings of IEEE International Conference on Systems, Man and Cybernetics*, Vol. 3, pp. 2121–2127.
[26] Sekmen, A. S., Wilkes, M., and Kawamura, K., 2002, "An Application of Passive Human-Robot Interaction: Human Tracking Based on Attention Distraction," IEEE Trans. Syst., Man Cybern., Part A, Syst. Humans, **32**, pp. 248–259.
[27] Shiomi, M., Kanda, T., Miralles, N., Miyashita, T., Fasel, I., Movellan, J., and Ishiguro, H., 2004, "Face-to-Face Interactive Humanoid Robot," *Proceedings of IEEE/RSJ International Conference on Intelligent Robots and Systems*, Vol. 2, pp. 1340–1346.
[28] Breazeal, C., 2004, "Function Meets Style: Insights From Emotion Theory Applied to HRI," IEEE Trans. Syst., Man, Cybern., Part C: Appl. Rev., **34**(2), pp. 187–194.
[29] Sucontphunt, T., Mo., Z., Neumann, U., and Deng, Z., 2008, "Interactive 3D Facial Expression Posing Through 2D Portrait Manipulation," Graphics Interface Conference, Windsor, Ontario, Canada, May 28–30.
[30] Jaeckel, P., Campbell, N., and Melhuish, C., 2008, "Facial Behaviour Mapping From Video Footage to a Robot Head," Rob. Auton. Syst., **56**, pp. 1042–1049.
[31] Pantic, M., and Rothkrantz, L., 2000, "Automatic Analysis of Facial Expressions: The State of the Art," IEEE Trans. Pattern Anal. Mach. Intell., **22**, pp. 1424–1445.
[32] Trezopoulos, D., and Waters, K., 1990, "Physically-Based Facial Modeling, Analysis, and Animation," J. Visualization Comput. Anim., **1**, pp. 73–80.
[33] Fukuda, T., Jung, M. J., Nakashima, M., Arai, F., and Hasegawa, Y., 2004, "Facial Expressive Robotic Head System for Human-Robot Communication and Its Application in Home Environment," Proc. IEEE, **92**(11), pp. 1851–1865.
[34] Hubert, J., and Merlet, J.-P., 2009, "Static of Parallel Manipulators and Closeness to Singularity," ASME J. Mech. Rob., **1**, p. 011011.
[35] Myszka, D. H., Murray, A. P., and Schmiedeler, J. P., 2009, "Singularity Analysis of an Extensible Kinematic Architecture: Assur Class N, Order N-1," ASME J. Mech. Rob., **1**, p. 011009.
[36] Park, F. C., and Kim, J. W., 1999, "Singularity Analysis of Closed Kinematic Chains," ASME J. Mech. Des., **121**, pp. 32–38.
[37] Weiguo, W., Qingmei, M., and Yu, W., 2004, "Development of the Humanoid Head Portrait Robot System With Flexible Face and Expression," *Proceedings of IEEE International Conference on Robotics and Biomimetics, ROBIO*, pp. 757–762.
[38] Allison, B., Nejat, G., and Kao, E., 2009, "The Design of an Expressive Humanlike Socially Assistive Robot," ASME J. Mech. Rob., **1**(1), pp. 1–8.
[39] Itoh, K., Miwa, H., Onishi, Y., Imanishi, K., Hayashi, K., and Takanishi, A., 2005, "Development of Face Robot to Express the Individual Face by optimizing the Facial Features," *Proceedings of 5th IEEE-RAS International Conference on Humanoid Robots*, pp. 412–417.
[40] Tadesse, Y., and Priya, S., 2011, "Determination of the Sinking and Terminating Points of Action Unit on Humanoid Skull Through GFEAD," *Proceedings of the SPIE*, Y. Bar-Cohen, and F. Carpi, eds., Vol. 7976, 79761V.
[41] Hanson, D., Bergs, R., Tadesse, Y., White, V., and Priya, S., 2006, "Enhancement of EAP Actuated Facial Expressions by Designed Chamber Geometry in Elastomers," *Proceedings of the SPIE*, Y. Bar-Cohen, ed., Vol. 6168, pp. 49–57.